Multi objective operation optimization method for flexible resources in industrial parks considering multiple uncertainties of source and load

Wei Liu[1*], Zilong Song[1], Lu Li[1], Jiaming Zhou[1], Yongming Liu[1], Xinli Chang[1]
[1]Weihai Power Supply Company, State Grid Shandong Electric Power Company, Weihai 264200, China
Corresponding author: Wei Liu (e-mail: lxl2025123@126.com).

ABSTRACT With the large-scale integration of distributed renewable energy and the increasing volatility of electric and gas loads, traditional deterministic models struggle to accurately characterize the dynamic response behavior of park-level energy systems. To address this issue, this paper proposes a multi-objective operation optimization methodology for park-level flexible resources that accounts for multiple source–load uncertainties. First, an empirical distribution is constructed based on historical source–load forecast error data, and a probability ambiguity set containing the true distribution is formulated using the Wasserstein distance to characterize the multiple uncertainties in both source and load. Second, a min–max distributionally robust optimization model is established with operational cost and carbon emissions as objectives, where the minimization problem corresponds to the search for the optimal operation scheme, and the maximization problem identifies the worst-case probability distribution within the ambiguity set. Furthermore, the model is transformed into a finite-dimensional convex optimization form using strong duality theory, and a weighted fuzzy membership degree method is introduced to achieve an equivalent solution. Simulation results demonstrate that the proposed methodology can effectively balance economy, environmental sustainability, and robustness, providing a credible decision-making tool for the optimal dispatch of flexible resources in park-level systems under data-limited scenarios.

INDEX TERMS Source–grid–load–storage; robust optimization; Wasserstein distance; flexible resources

I. INTRODUCTION

Under the strategic goals of carbon peaking and carbon neutrality, industrial parks are accelerating the construction of energy supply systems centered on renewable energy and characterized by multi-energy complementarity[1-3]. However, the output of renewable sources such as wind and photovoltaic power exhibits strong randomness and intermittency due to meteorological conditions, while the diverse load demands, including electricity and heat within the park, also fluctuate significantly with production schedules and user behaviors[4], and the deep coupling of these multiple uncertainties on both the source and load sides can readily lead to power mismatches and degradation of supply reliability, posing severe challenges to the safe and economic operation of park-level integrated energy systems. Flexible resources, such as energy storage, adjustable loads, and electric vehicles, possess rapid response capabilities and power regulation flexibility, making them one of the key means to smooth source-load fluctuations and maintain real-time system balance[5-7]. Nevertheless, because the distribution characteristics of source-load prediction errors are difficult to characterize accurately, how to fully exploit the synergistic potential of multiple types of flexible resources under uncertainty while simultaneously balancing the economic and environmental performance of park operation has become a pressing modeling challenge in the field of optimal dispatch for industrial parks. Therefore, investigating multi-objective optimal operation methods for flexible resources that account for multiple source-load uncertainties holds significant importance and practical engineering value[8-9].

The treatment of source-load uncertainties in park-level dispatch primarily falls into two categories: stochastic optimization (SO) [10] and robust optimization (RO) [11]. SO assumes that prediction errors follow specific probability distributions, and then converts the uncertain problem into deterministic scenarios via Monte Carlo sampling or scenario generation and reduction techniques, thereby obtaining an economically optimal schedule in the expected sense[12-13]. However, its performance critically depends on the prior distribution assumption, which is often hard to acquire accurately due to limited historical data or incomplete statistics. In contrast, RO characterizes the fluctuation ranges of source-load parameters via uncertainty sets and seeks dispatch strategies that remain feasible under the worst-case realization, thus requiring no probabilistic information and ensuring robust safety[14-16]. Yet this method focuses solely on extreme boundary scenarios while completely discarding probability information, leading to overly conservative solutions with high expected operating costs and poor economic performance. In summary, SO is vulnerable to distributional misspecification, whereas RO abandons probabilistic information by fixating on worst-case extremes, resulting in excessive conservatism—both approaches struggle to strike an effective balance between economic optimality and robust security, as they represent two extremes in utilizing distributional information versus resisting uncertainty.

In recent years, distributionally robust optimization (DRO) has emerged as a research hotspot in optimization under uncertainty[17-19]. Instead of assuming a single probability distribution, DRO posits that the true distribution resides within an ambiguity set constructed from historical data, and optimizes the expected performance under the worst-case distribution within that set—thereby combining the advantage of stochastic optimization in utilizing distributional information with the capability of robust optimization to hedge against distributional uncertainty. Early DRO studies typically constructed ambiguity sets using Kullback-Leibler (KL) divergence or total variation distance[20-21]; however, such distance metrics require all candidate distributions to share the same support set as the empirical distribution, rendering them incapable of accommodating new samples that may arise in practice and thus limiting their generalization ability. In recent years, the Wasserstein distance, rooted in optimal transport theory, has attracted considerable attention[22-23]. Unlike KL divergence, the Wasserstein distance can measure discrepancies between distributions defined on different support sets, and the ambiguity sets constructed thereby enjoy favorable finite-sample guarantees and out-of-sample generalization performance—as the historical sample size tends to infinity, the ambiguity set shrinks to the true distribution with probability one, manifesting a distinct data-driven character. Reference [24] proposes a Wasserstein-distance-based distributionally robust chance-constrained optimal reactive power dispatch model for active distribution networks under renewable output uncertainty, and validates its effectiveness via simulations on 123-bus systems. However, the use of this approach in multi-objective scheduling for park-level integrated energy systems is still limited, especially with respect to coordinating diverse flexible resources and developing a distributionally robust dispatch framework that jointly optimizes economic cost and carbon emissions.

In summary, to address the challenges of precisely characterizing distributional information and effectively balancing economic performance with robustness in flexible resource dispatch under multiple source-load uncertainties, this paper proposes a distributionally robust multi-objective optimal dispatch model based on a Wasserstein ambiguity set. Driven by historical data of source-load prediction errors, the ambiguity set is constructed and embedded into a two-stage min-max distributionally robust optimization framework. The model is then reformulated into a tractable deterministic convex optimization problem via strong duality theory, and the weighted fuzzy membership method is employed to obtain the economic-environmental Pareto frontier. Simulation results demonstrate that the proposed approach achieves a superior trade-off among economy, environmental friendliness, and robustness, providing a credible decision-making tool for optimal flexible resource dispatch in industrial parks under data-limited scenarios.

II. PARK-LEVEL INTEGRATED ENERGY SYSTEM

The park-level integrated energy system (PIES) is structured around electric, thermal, and natural gas buses, which serve as the central hubs. Through coupling devices such as gas turbines and heat pumps, the system enables electric–thermal–gas multi-energy complementarity and engages in bidirectional energy exchange with the external power grid and natural gas network. On the source side, distributed renewable energy resources, including wind turbines and photovoltaic (PV) arrays, are deployed. On the storage side, both electric and thermal energy storage devices are installed. On the load side, diverse electric and thermal loads as well as demand response (DR) resources are integrated. This configuration establishes a source– grid–load–storage interactive paradigm for the park, as illustrated in Figure 1. In the day-ahead scheduling stage, the dispatch center determines the output schedule of each controllable device and the dispatch baseline of flexible resources based on source–load forecast information. In the real-time operation stage, when deviations arise between the actual and forecasted source–load values, real-time power balance is maintained by adjusting the charging/discharging power of energy storage systems, demand response loads, and the power exchanged with the external grid.

A. SYSTEM DEVICE MODELING

The gas turbine serves as the core combined heat and power (CHP) device in the park. By consuming natural gas, it simultaneously generates electricity and high-temperature waste heat. Its energy conversion relationship can be expressed as follows:

$$P_t^{GT} = \eta_e G_t^{GT} q_{gas}, \qquad H_t^{GT} = \eta_h G_t^{GT} q_{gas}$$

Where P_t^{GT} and H_t^{GT} denote the electric output and thermal output of the gas turbine, respectively; G_t^{GT} represents the natural gas consumption during period t; q_{gas} is the calorific value of natural gas (kWh/m^3); and η_e and η_h denote the power generation efficiency and waste heat recovery efficiency, respectively.

The gas turbine output must satisfy the capacity constraint and ramping constraints:

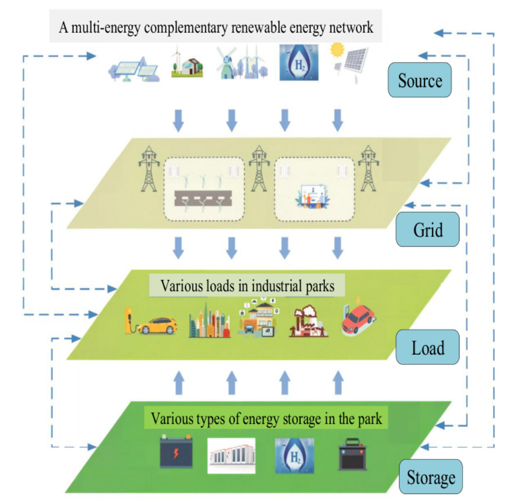

FIGURE 1. Source-grid-load-storage interaction mode in the park

$$0 \le P_t^{GT} \le P_{\max}^{GT}, \qquad -R_{down} \le P_t^{GT} - P_{t-1}^{GT} \le R_{up}$$

where $P_{\max}^{GT}$ represents the rated electric power; R_{down} and R_{up} denote the upward and downward ramping rate limits, respectively.

The heat pump extracts thermal energy from a low-temperature heat source by consuming electricity and constitutes another key electric–thermal coupling device in the park. The relationship between its heating output and electricity consumption is given by:

$$H_t^{HP} = COP \cdot P_t^{HP}$$

where COP denotes the coefficient of performance for heating, and P_t^{HP} represents the electric power consumption of the heat pump, which is subject to its rated power limit.

The operational characteristics of electric and thermal energy storage systems are uniformly described by the following generalized model, which includes the state-of-energy equation and charging/discharging power constraints:

$$E_{t+1}^s = E_t^s(1-\sigma_s) + \left(P_t^{ch}\eta_{ch} - \frac{P_t^{dis}}{\eta_{dis}}\right)\Delta t$$
$$0 \le P_t^{ch} \le u_t^s P_{\max}^{ch}, \quad 0 \le P_t^{dis} \le (1-u_t^s)P_{\max}^{dis}$$

where E_t^s denotes the stored energy (kWh); P_t^{ch} and P_t^{dis} represent the charging and discharging power, respectively; u_t^s is the charging/discharging state indicator (a 0–1 variable) used to prevent simultaneous charging and discharging; σ_s denotes the self-discharge loss coefficient; and η_{ch} and η_{dis} represent the charging and discharging efficiencies, respectively.

Meanwhile, the storage capacity must be maintained within the safe operating range:

$$E_{\min}^s \le E_t^s \le E_{\max}^s$$

The park is connected to the external power grid and natural gas network via tie lines and gas pipelines, and the exchanged power must satisfy the following constraints:

$$P_{\min}^{grid} \le P_t^{grid} \le P_{\max}^{grid}, \qquad G_{\min}^{gas} \le G_t^{gas} \le G_{\max}^{gas}$$

where the natural gas consumption G_t^{GT} and the purchased gas volume G_t^{gas} satisfy the balance relationship.

In addition, the electric bus must ensure real-time balance between generation and consumption:

$$P_t^{GT} + P_t^{PV} + P_t^{WT} + P_t^{dis} + P_t^{grid} = P_t^{ch} + P_t^{HP} + P_t^{L} + \sum_j \Delta P_{j,t}^{FL}$$

The thermal bus balance constraint is expressed as:

$$H_t^{GT} + H_t^{HP} + H_t^{HS,dis} = H_t^{HS,ch} + H_t^{L} + \sum_j \Delta H_{j,t}^{FL}$$

where P_t^{PV} and P_t^{WT} denote the forecasted output of photovoltaic and wind power, respectively; P_t^L and H_t^L represent the forecasted electric and thermal loads, respectively; and $\Delta P_{j,t}^{FL}$ and $\Delta H_{j,t}^{FL}$ denote the load adjustment amounts of various flexible resources, whose adjustable ranges are determined by the flexible resource model presented in Section 2.2. The renewable energy output and load demand appearing in the above power balance constraints are all expressed in the form of forecasted values, thereby providing a benchmark for the introduction of uncertainty modeling and distributionally robust optimization.

B. FLEXIBLE RESOURCE ADJUSTABLE POTENTIAL MODEL

The flexible resources in the park mainly include shiftable loads, interruptible loads, and electric vehicle (EV) clusters. Unlike conventional rigid loads, flexible resources possess an adjustable power range within specific time intervals and can provide upward or downward regulation capability when system power imbalance occurs. This section presents their adjustable potential models and response cost functions.

(1) Shiftable Loads

Shiftable loads refer to load types whose electricity consumption time can be shifted as a whole within a certain range, provided that the total energy consumption remains unchanged, such as certain industrial production lines, disinfection and cleaning equipment, etc.

Let the continuous working duration of shiftable load L_s be D_s time intervals. A 0–1 start-up state variable $v_{s,t}$ is introduced, and its constraint is expressed as:

$$\sum_{t=t_s^{start}}^{t_s^{end}} v_{s,t} = D_s, \qquad t \in [t_s^{start}, t_s^{end}]$$

where the load adjustment amount $\Delta P_{j,t}^{FL}$ in period t equals the difference between the shifted load of the start-up state in that period and the baseline electricity consumption. The specific expression is determined according to the load distribution before and after the shifting. Shiftable loads do not alter the total electricity consumption and therefore incur no additional operational cost.

(2) Interruptible Loads

Interruptible loads allow partial curtailment when the system power supply is under strain, and corresponding economic compensation must be provided after the demand response event concludes.

Let the rated power of interruptible load L_c be P_c^{rated}, and let the maximum curtailment ratio in period t be $\alpha_c^{\max}$. The curtailment amount then satisfies:

$$0 \leq \Delta P_{c,t}^{FL} \leq \alpha_c^{\max} P_c^{rated}$$

Accordingly, the demand response compensation cost in period t is given by:

$$C_{c,t}^{DR} = c_c^{cut} \cdot \Delta P_{c,t}^{FL}$$

where c_c^{cut} denotes the compensation price per unit of curtailed electricity.

(3) Electric Vehicle Clusters

Electric vehicles integrated into the park at scale can be regarded as distributed mobile energy storage resources. A certain number of electric vehicles are aggregated into a virtual energy storage unit, whose aggregated state-of-energy evolution equation is expressed as:

$$E_{t+1}^{EV} = E_t^{EV} + \left(P_t^{EV,ch} \eta_{EV} - \frac{P_t^{EV,dis}}{\eta_{EV}} \right) \Delta t - E_t^{trip}$$

where E_t^{EV} denotes the aggregated energy of the cluster; $P_t^{EV,ch}$ and $P_t^{EV,dis}$ represent the aggregated charging and discharging power, respectively; η_{EV} is the charging/discharging efficiency; and E_t^{trip} denotes the energy consumed by vehicles departing from the grid for travel. The aggregated charging and discharging power is constrained by the connection capacity and battery status:

$$\begin{cases} 0 \leq P_t^{EV,ch} \leq P_{\max}^{EV,ch}, \\ 0 \leq P_t^{EV,dis} \leq P_{\max}^{EV,dis}, \\ E_{\min}^{EV} \leq E_t^{EV} \leq E_{\max}^{EV}. \end{cases}$$

The EV cluster participates in system power regulation by adjusting its charging and discharging periods. The regulation cost primarily manifests as battery cycling degradation, which can be equivalently incorporated into the operation and maintenance cost term.

III. SOURCE–LOAD UNCERTAINTY MODELING BASED ON WASSERSTEIN METRIC

A. EMPIRICAL DISTRIBUTION OF SOURCE–LOAD FORECAST ERRORS

The source–load uncertainty in the park primarily originates from the fluctuations in wind turbine and photovoltaic output and the stochastic variations in electric and thermal load demand. The actual source–load values are expressed as the superposition of the day-ahead forecasted values and the forecast errors:

$$\begin{aligned} P_t^{WT} &= \widehat{P}_t^{WT} + \xi_t^{WT}, & P_t^{PV} &= \widehat{P}_t^{PV} + \xi_t^{PV}, \\ P_t^{load} &= \widehat{P}_t^{load} + \xi_t^{P}, & H_t^{load} &= \widehat{H}_t^{load} + \xi_t^{H}. \end{aligned}$$

where $\widehat{P}_t^{WT}$, $\widehat{P}_t^{PV}$, $\widehat{P}_t^{load}$, and $\widehat{H}_t^{load}$ denote the day-ahead forecasted values; ξ_t^{WT}, ξ_t^{PV}, ξ_t^{P}, and ξ_t^{H} represent the corresponding forecast errors.

The four types of forecast errors over the entire dispatch period T are stacked into a random vector ξ.

Based on N historical forecast error samples $\{\widehat{\xi}_i\}_{i=1}^N$, the empirical probability distribution is constructed as follows:

$$\widehat{P}_N = \frac{1}{N} \sum_{i=1}^{N} \delta_{\widehat{\xi}_i}$$

where $\delta_{\widehat{\xi}_i}$ denotes the Dirac measure at the sample point $\widehat{\xi}_i$. This empirical distribution serves as the data foundation for constructing the Wasserstein ambiguity set.

B. CONSTRUCTION OF THE WASSERSTEIN AMBIGUITY SET

For two probability distributions P and Q defined on the support set Ξ, their p-Wasserstein distance is defined as:

$$W_p(P,Q) = \inf_{\Pi \in \Xi} \left\{ \left(\int_{\Xi \times \Xi} \|\xi - \xi'\|^p \Pi(d\xi, d\xi') \right)^{1/p} \right\}$$

where Π denotes the joint distribution of the probability distributions P and Q. In this paper, the 1-Wasserstein distance $p = 1$ is adopted, as its dual linear programming form facilitates subsequent model transformation.

Centered at the empirical distribution $\widehat{P}_N$, the Wasserstein ambiguity set with radius ε is constructed as follows:

$$\Gamma_\varepsilon(\widehat{P}_N) = \{ P \in M(\Xi) : W_1(P, \widehat{P}_N) \leq \varepsilon \}$$

where $M(\Xi)$ denotes the space of all probability distributions on the support set Ξ. This ambiguity set characterizes that the true but unknown probability distribution P^* of the source–load forecast errors falls within the Wasserstein ball with a high confidence level.

The radius ε of the ambiguity set controls the degree of conservatism of the model. An excessively small radius may fail to contain the true distribution, rendering the model overly optimistic, whereas an excessively large radius leads to excessive conservatism, sacrificing economic performance. Based on the mean-rate convergence theory, given a confidence level $\beta \in (0,1)$, the radius is selected according to the following formula:

$$\varepsilon(\beta, N) = C \cdot N^{-1/\max\{d,2\}}$$

where d denotes the dimensionality of the forecast error vector, and C is a coefficient associated with the confidence level β, which can be determined through theoretical derivation or data-driven methods. This selection approach ensures that the radius tends to zero as the sample size N increases, and that the true distribution falls within the ambiguity set with a probability no lower than β, thereby fully embodying the data-driven modeling characteristics.

IV. PARK-LEVEL DISTRIBUTIONALLY ROBUST MULTI-OBJECTIVE OPTIMAL DISPATCH MODEL

A. TWO-STAGE DISTRIBUTIONALLY ROBUST MODEL FORMULATION

Based on the deterministic system model and the source–load Wasserstein ambiguity set, this section establishes a two-stage distributionally robust optimal dispatch model that accounts for both economic performance and environmental sustainability.

(1) Objective Function

To address the source–load uncertainty, the dispatch decisions are divided into two stages:

In the first stage (day-ahead), the baseline dispatch schedule is formulated before the uncertainty is revealed, including the gas turbine output, baseline charging/discharging power of energy storage, contracted power exchanged with the external grid, and day-ahead dispatch instructions for demand response resources.

In the second stage (real-time), once the actual source–load values are observed, the real-time operating points of flexible resources are adjusted to maintain power balance, and the corresponding adjustment costs are incurred.

Let the vector of first-stage decision variables be denoted by x, and the vector of second-stage decision variables be denoted by $y(\xi)$.

The model simultaneously considers two optimization objectives: operational cost and carbon emissions. Under the distributionally robust framework, the expected values under the worst-case probability distribution within the Wasserstein ambiguity set are adopted as the optimization criteria for each objective. The operational cost C_{op} includes fuel cost, electricity purchase cost, equipment operation and maintenance (O&M) cost, demand response compensation cost, and real-time imbalance penalty cost. The carbon emission cost C_{em} accounts for both the direct emissions from natural gas consumption by the gas turbine and the equivalent carbon flow associated with purchased electricity. The expressions are as follows:

$$
\begin{aligned}
C_{op} = \sum_{t \in T} \Big(& c_{gas} G_t^{GT} + c_t^{grid} P_t^{grid} + c_{OM} P_t^{GT} \\
& + \sum_{c} c_c^{cut} \Delta P_{c,t}^{FL} + \lambda^{pen} |P_t^{imb}| \Big)
\end{aligned}
$$

$$
C_{em} = \sum_{t \in T} \left(\mu_{gas} G_t^{GT} + \mu_{grid} P_t^{grid} \right)
$$

where c_{gas} and c_t^{grid} denote the natural gas price and the time-of-use electricity price, respectively; c_{OM} represents the unit O&M cost; λ^{pen} is the imbalance power penalty coefficient; μ_{gas} and μ_{grid} denote the carbon emission coefficients; and P_t^{grid} represents the actual power exchanged with the external grid.

(2) System Constraints

The first-stage constraints include device capacity limits, ramping constraints, energy storage state equations, and the upper bounds for day-ahead demand response dispatch, which are consistent with the deterministic model presented in Section 1. The second-stage constraints require that, on the basis of the first-stage decisions, for any forecast error realization ξ, there exists a feasible real-

time adjustment scheme that satisfies the power balance and the adjustment capability limits of the devices.

The above two-stage constraints are uniformly denoted as $x \in \theta$ and $y(\xi) \in \vartheta(x, \xi)$. In summary, the two-stage distributionally robust optimal dispatch model can be compactly formulated as follows:

$$
\min_{x \in \theta} \max_{P \in \Gamma_\varepsilon(\widehat{P}_N)} E_P \left[\min_{y \in \vartheta(x,\xi)} c(x, y, \xi) \right]
$$

Substituting the operational cost C_{op} or the carbon emission cost C_{em} into the above expression yields the optimization model for the corresponding objective. The inner min–max–max structure of the model reveals its distributionally robust characteristics: the inner max searches for the worst-case distribution within the ambiguity set, the middle min optimizes the real-time dispatch cost under a given distribution, and the outer min seeks the optimal day-ahead scheme under the worst-case expectation derived from the preceding layers.

B. MODEL DUAL TRANSFORMATION AND MULTI-OBJECTIVE SOLUTION

The min–max–min structure involves an infinite-dimensional search over the probability distribution, which constitutes a semi-infinite optimization problem that is difficult to solve directly. In this paper, the Kantorovich–Rubinstein duality theorem for the Wasserstein distance is employed to perform an equivalent transformation. With the first-stage decision x fixed, the inner worst-case expectation problem can be equivalently transformed into:

$$
\begin{aligned}
& \min_{\lambda_\varepsilon \geq 0} \lambda_\varepsilon + \frac{1}{N} \sum_{i=1}^{N} \sup_{\xi \in \Xi} \left[Q(x, \xi) - \lambda \|\xi - \widehat{\xi}_i\| \right] \\
& Q(x, \xi) = \min_{y \in \vartheta(x,\xi)} c(x, y, \xi)
\end{aligned}
$$

where $Q(x, \xi)$ denotes the optimal real-time adjustment cost given the first-stage decision and the forecast error.

Furthermore, for each historical sample, an auxiliary variable s_i is introduced to replace the corresponding supremum term. By applying the linear programming duality theory, the inner supremum can be transformed into a set of deterministic linear constraints. Ultimately, the original two-stage distributionally robust problem is equivalently converted into a single-level deterministic convex optimization problem:

$$\begin{aligned} &\min_{x,\lambda_\varepsilon,s_i} \ \lambda_\varepsilon + \frac{1}{N}\sum_{i=1}^{N} s_i \\ &\text{s.t.} \quad s_i \geq C_{op}(x,\xi_i'), \quad \forall i,\ \forall \xi_i' \in \bar{\Xi}_i \end{aligned}$$

where ξ_i' represents the perturbation point around the i-th historical sample. The transformed model assumes the form of a linear program or a second-order cone program, which can be efficiently solved by directly invoking mature solvers such as CPLEX and Gurobi.

After the transformation, the deterministic optimization objectives $F_1(x,\lambda_1,s_{1i})$ and $F_2(x,\lambda_2,s_{2i})$ are obtained for the operational cost and carbon emissions, respectively. To obtain the Pareto front, the weighted fuzzy membership degree method is adopted. The single-objective optimal values $F_1^{\min}$ and $F_2^{\min}$ for the two objectives are first solved separately, along with their respective upper bounds $F_k^{\max}$. For each objective, a linear fuzzy membership function is defined as follows:

$$C_{em} = \sum_{t\in T}\left(\mu_{gas}G_t^{GT} + \mu_{grid}P_t^{grid}\right)$$

On this basis, a weighted sum of satisfaction maximization problem is constructed:

$$\max \ \omega_1\mu_1(F_1) + \omega_2\mu_2(F_2)$$

where the weights satisfy $\omega_1,\omega_2 \geq 0$ and $\omega_1+\omega_2 = 1$. By traversing the weight combinations and solving the above deterministic optimization problem, a series of Pareto optimal solutions can be obtained, constituting the Pareto front under the economic–environmental dual-objective framework, thereby providing a reference for different decision-making preferences.

V. CASE STUDY

A. CASE SETTING

Based on an industrial park as the simulation object, the effectiveness of the proposed distributionally robust multi-objective optimal dispatch model is validated. The park, primarily housing electronic information manufacturing and supporting equipment processing enterprises, has established an electric-thermal coupled integrated energy system equipped with gas turbines, heat pumps, electrical and thermal energy storage units, and integrated with distributed renewable energy sources including wind power and photovoltaics. The peak electrical and thermal loads of the park are approximately 16,800 kW and 14,900 kW, respectively. The park incorporates two wind farms with a total installed capacity of 3 MW, and distributed photovoltaic stations with

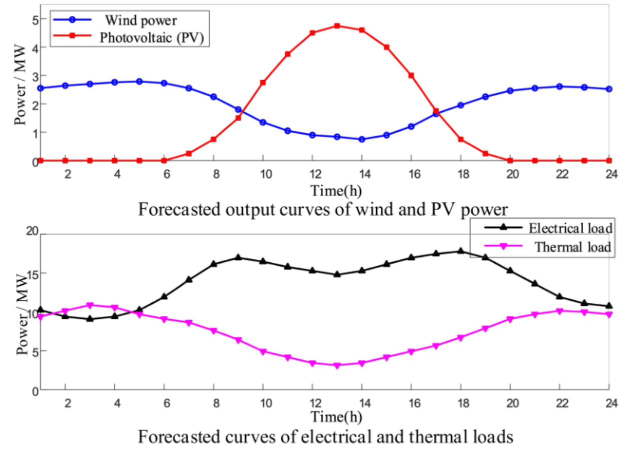

FIGURE 2. Forecast curves of wind power, photovoltaic power, electric load, and heat load

TABLE 1. Main equipment parameters and energy prices

Parameter	Value	Parameter	Value
Rated electrical power of gas turbine	8000 kW	Electric storage rated capacity	3000 kWh
Power generation efficiency / Waste heat recovery efficiency	0.35/0.45	Max charge/discharge power (electric storage)	600 kW
Rated heating power of heat pump	4000 kW	Thermal storage rated capacity	2000 kWh
COP of heat pump (Coefficient of Performance)	3.5	Charge/discharge efficiency	0.95
Maximum exchange power of tie-line	5000 kW	Peak/flat/valley tariffs	0.95/0.65/0.35 yuan//kWh
Price of natural gas	2.5 yuan/m^3	Calorific value of natural gas	9.7 kWh/m^3
Carbon emission factor of gas turbine	0.20 kg/kWh	Carbon emission factor of purchased electricity	0.75 kg/kWh

a total installed capacity of 5 MW. The dispatch horizon spans 24 hours with a time step of one hour. The typical daily output forecasts for wind and photovoltaic power, along with the electrical and thermal load forecasts, are illustrated in Figure 2. The primary equipment parameters and energy prices are summarized in Table 1.

The flexible resources in the park include interruptible loads, shiftable loads, and an electric vehicle (EV) aggregation. The interruptible loads have a total rated power of 2500 kW, with a maximum interruptible ratio of 30% and a compensation price of 0.5 yuan/kWh. The shiftable loads have a total rated power of 1800 kW, are allowed to operate within the time window of 06:00–22:00, and require a continuous operating duration of 4 hours. The EV aggregation has an aggregated capacity of 1200 kWh and a maximum charging/discharging power of 300 kW.

For uncertainty modeling, the number of historical samples for the four types of forecast errors is $N = 500$, obtained from the actual operational data of the park over the past two years. The radius of the Wasserstein ambiguity

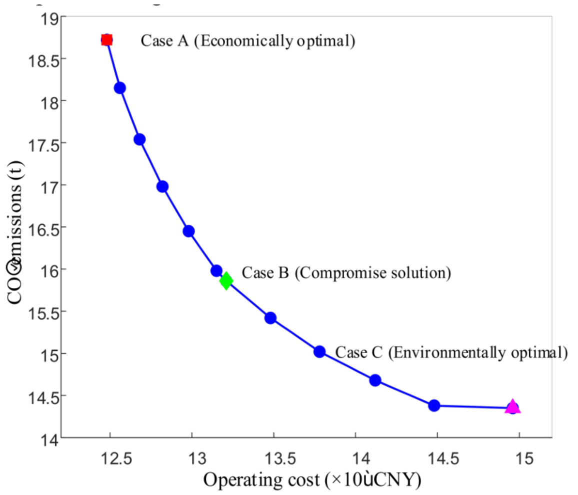

FIGURE 3. Economic-environmental bi-objective Pareto front

set is set to $\varepsilon = 0.038$, with a confidence level of $\beta = 0.95$. The model is programmed in MATLAB R2023a and solved using CPLEX. The Pareto frontier is generated by solving the model 21 times, sweeping the weight coefficient ω_1 from 0 to 1 with a step size of 0.05.

B. OPTIMIZATION RESULTS AND PARETO FRONTIER ANALYSIS

Based on the system parameters specified in Table 1 and the source-load forecast data, the distributionally robust multi-objective optimal dispatch model is solved to obtain the Pareto optimal solution set under the dual economic and environmental objectives, and the dispatch strategies of typical solutions are comparatively analyzed.

By sweeping the weight coefficient from 0 to 1 with a step size of 0.05, the deterministically equivalent optimization problem is solved 21 times, yielding a series of Pareto optimal solutions that constitute the Pareto frontier depicted in Figure 3.

As observed, there is a pronounced negative correlation between the park's operating cost and carbon emissions. The Pareto frontier is globally convex toward the origin, indicating a diminishing marginal rate of substitution between the two objectives—that is, the economic cost required to reduce each additional unit of carbon emissions increases progressively as the emission level declines. At the two extreme endpoints of the frontier, the economically optimal solution (Solution A) achieves a total operating cost of CNY 124,800 with corresponding carbon emissions of 18.72 t, while the environmentally optimal solution (Solution C) attains carbon emissions of 14.35 t with an operating cost of CNY 149,600. The cost difference between these two extreme schemes is approximately 20%, while the emissions differ by about 23%. The compromise solution (Solution B) yields an operating cost of CNY 132,100 and carbon emissions of 15.86 t, achieving a favorable overall balance. This result indicates that there exists a substantial decision space between economic performance and environmental friendliness, and the proposed model can provide decision-makers with distinct preferences with a clear basis for Pareto-optimal selection.

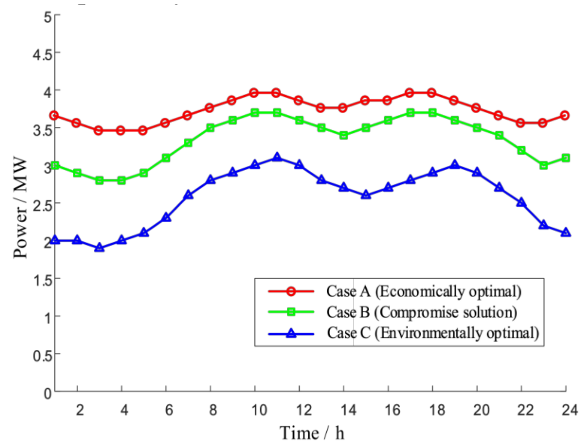

FIGURE 4. Comparison of gas turbine output under three schemes

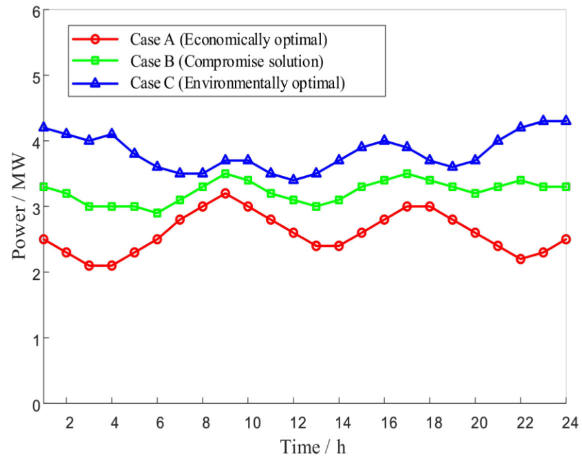

FIGURE 5. Comparison of external power purchase under three schemes

To further reveal the underlying mechanism through which different objective preferences influence the system dispatch decisions, the aforementioned three representative solutions are selected for comparative analysis. Under the multi-energy complementary architecture of the park, the gas turbine serves as both the core power supply unit and the primary source of carbon emissions, while power purchased from the external grid constitutes its most direct substitute. The power dispatch between these two sources fundamentally determines the economic-environmental trade-off. Accordingly, this section centers the comparison on two key decision variables: the gas turbine output and the purchased electricity power. Figure 4 and Figure 5 present the hourly gas turbine outputs and the hourly purchased electricity powers under the three schemes, respectively.

The gas turbine output curves under the three schemes exhibit notable differences in both shape and magnitude, reflecting the impact of distinct objective preferences on dispatch strategies. Solution A maintains a consistently high and smooth output throughout the day, fully exploiting the economic advantage of natural gas generation while reducing power purchases from the grid during peak and flat periods. Solution C displays a pronounced bimodal pattern, with output rising moderately during the midday and evening peaks to ensure reliability, while dropping to lower levels during nighttime off-peak hours to minimize direct carbon emissions from fossil fuels. Solution B lies between the two, with peak-hour output approaching that of Solution A while off-peak output falls markedly below that of Solution A but remains higher than that of Solution C, embodying a balanced trade-off between economy and environmental protection. The corresponding gas turbine utilization hours under the three schemes are 12.2 h, 10.2 h, and 7.7 h, respectively, showing a significant disparity.

As the primary substitute for the gas turbine, purchased electricity exhibits an opposing dispatch trend. As shown in Figure 5, the purchased power under Solution C consistently exceeds that under Solutions A and B throughout the day, particularly during flat and off-peak tariff periods, where additional electricity is procured to replace gas turbine generation and thereby reduce direct emissions. Solution A has the lowest purchased power, used mainly for peak-valley leveling and real-time regulation margins, with most load met by the gas turbine. Solution B falls in between. The total purchased electricity under the three schemes amounts to 62,100 kWh, 78,500 kWh, and 96,800 kWh, respectively, reflecting the significant differences in primary power source selection under varying objective preferences.

Regarding flexible resource deployment, the total charging and discharging volumes of electrical and thermal energy storage remain broadly similar across the three schemes, confirming that storage plays an indispensable role in peak shaving and valley filling regardless of preference. The heat pump output exhibits a complementary relationship with the waste heat from the gas turbine: under Solution A, the heat load is predominantly met by waste heat, with the heat pump serving as a supplement; under Solution C, waste heat is substantially reduced, and the heat pump assumes the majority of heat supply. Demand response calls increase under Solution C to maintain power balance under reduced fossil fuel consumption. Table 2 summarizes the key operational metrics of the three schemes.

It can be observed that the differences in scheduling strategies under different objective preferences are mainly reflected in the output distribution between gas turbines and purchased electricity: the economic preference drives the system to increase the output of gas turbines and reduce purchased electricity, while the environmental preference drives the opposite scheduling direction. The proposed model can achieve a flexible trade-off between economic and environmental objectives under the premise of satisfying operational constraints by rationally configuring the output proportion of the two types of main power sources and combining the coordinated regulation of flexible resources such as energy storage and demand response.

TABLE 2. Comparison of key operational indicators under three typical schemes

Index	Value	Parameter	Value
Total Operating Cost (10^4 Yuan)	12.48	13.21	14.96
Total Carbon Emission (ton)	18.72	15.86	14.35
Utilization Hours of Gas Turbine (h)	18.6	15.2	10.8
Natural Gas Consumption ($10^4 \cdot m^3$)	4.85	3.96	3.24
Purchased Electricity Quantity ($10^4 \cdot$kWh)	6.42	8.15	10.38
Total Charge-Discharge Energy of Energy Storage ($10^4 \cdot$kWh)	1.28	1.31	1.33
Dispatching Volume of Demand Response ($10^4 \cdot$kWh)	0.43	0.56	0.68

TABLE 3. Comparison of optimization results under three methods

Index	Stochastic Optimization	Robust Optimization	Proposed Method
Expected Operating Cost (10^4 Yuan)	12.18	14.52	13.21
Worst-Case Scenario Cost (10^4 Yuan)	16.85	14.95	15.28
Carbon Emission (ton)	17.24	15.42	15.86
Computation Time (s)	85.6	42.3	156.8

C. COMPARATIVE EXPERIMENTS AND ROBUSTNESS ANALYSIS

To verify the superiority of the distributionally robust optimization method proposed in this paper, it is compared with two traditional uncertainty handling methods, namely stochastic optimization and classical robust optimization. The three methods adopt identical park system parameters, source-load forecasting data, and historical sample sets of forecasting errors to ensure the fairness of the comparison.

Specifically, the stochastic optimization method generates 10 typical scenarios based on historical samples, with the goal of minimizing the expected operating cost while treating carbon emissions as a constraint. The classical robust optimization adopts a box uncertainty set to describe the deviation range of source and load, aiming to minimize the operating cost under the worst-case scenario. The proposed method in this paper simultaneously optimizes operating cost and carbon emissions, and selects the compromise satisfactory solution with $\omega_1 = \omega_2 = 0.5$ as the comparison scheme. The comparison indicators include expected operating cost, worst-case scenario cost, carbon emission amount, and computation time, and the results are presented in Table 3.

As can be seen from the table, the stochastic optimization achieves the optimal expected operating cost of 121,800 yuan, which is attributed to the fact that it is optimized directly based on the exact distribution assumption of historical samples, and the decision scheme is highly customized for the empirical distribution, thus obtaining the minimum average cost. However, when facing scenarios that deviate from the empirical distribution, its worst-case scenario cost reaches up to 168,500 yuan, about 9.3% higher than the proposed method, exposing its high sensitivity to the deviation of distribution assumptions. The classical robust optimization is oriented to the optimization of the most severe scenarios, which guarantees its resistance to extreme fluctuations. As a result, it achieves the optimal worst-case scenario cost of 149,500 yuan, but its expected operating cost is as high as 145,200 yuan, with a significant economic loss. The proposed method in this paper is close to the level of classical robust optimization in terms of worst-case scenario cost, while the expected operating cost is greatly reduced compared with robust optimization, and the carbon emission is also between the two, realizing a comprehensive balance of economy, robustness and environmental friendliness. In terms of computation time, the proposed method takes 156.8 seconds due to the involvement of dual transformation and multiple rounds of solving. Although it is higher than the other two methods, it is still within the acceptable range for engineering applications.

VI. CONCLUSION

Aiming at the issues that the probability distribution information is difficult to obtain accurately and the economy and robustness are hard to be effectively balanced in the scheduling of park flexible resources under multiple source-load uncertainties, this paper proposes a distributionally robust multi-objective optimal scheduling model based on the Wasserstein ambiguity set. Through theoretical analysis and case verification, the main conclusions are drawn as follows:

1) The probability distribution ambiguity set constructed based on the Wasserstein metric can characterize the distribution uncertainty of source-load forecasting errors in a data-driven manner, avoiding the dependence of traditional stochastic optimization on prior distribution assumptions. The established two-stage distributionally robust min-max model can be equivalently transformed into a deterministic convex optimization problem via the strong duality theory, which obtains a day-ahead scheduling scheme that balances economy and robustness while ensuring solving efficiency.

2) The comparison results with traditional stochastic optimization and robust optimization show that the proposed method achieves a better balance between the expected operating cost and the worst-case scenario cost, which verifies the applicability and superiority of distributionally robust optimization in the scheduling of park integrated energy systems. The economic-environmental Pareto frontier can provide a flexible selection basis for decision-makers with different preferences.

Acknowledgement: Not applicable.

Author Contributions: The authors confirm contribution to the paper as follows: Wei Liu, Zilong Song: Conceptualization, data curation, formal analysis; Lu Li, Jiaming Zhou, Yongming Liu: funding acquisition, investigation, methodology, project administration, resources, software; Xinli Chang: supervision, validation, visualization, writing—original draft, writing—review and editing. All authors reviewed the results and approved the final version of the manuscript.

Availability of Data and Materials: The data that support the findings of this study are available from the corresponding author on reasonable request.

Ethics Approval: Not applicable.

Conflicts of Interest: The authors declare no conflicts of interest to report regarding the present study.

Funding Statement: This work was supported by Science and Technology Project of State Grid Shandong Electric Power Company, (Key Technologies Research and Demonstration Application for Coordinated Control of Integrated Source-Grid-Load-Storage Parks and Regional Power Grids, No.: 520613250002).

REFERENCES

[1] J. Wei, Y. Zhang, J. Wang, et al., “Decentralized demand management based on alternating direction method of multipliers algorithm for industrial park with CHP units and thermal storage,” *J. Mod. Power Syst. Clean Energy*, vol. 10, no. 1, pp. 120–130, 2022, doi: 10.35833/MPCE.2020.000623.

[2] T. Wang and X. Yan, “Research on modeling and parameter identification of comprehensive load model of distribution network in industrial park,” *Chin. J. Electron.*, vol. 33, no. 1, pp. 264–273, 2024, doi: 10.23919/CJE.2022.00.024.

[3] J. Wang, Y. Shi, and Z. Yue, “Intelligent demand response for industrial energy management considering thermostatically controlled loads and EVs,” *IEEE Trans. Ind. Informat.*, vol. 15, no. 6, pp. 3432–3442, 2019, doi: 10.1109/TII.2018.2875866.

[4] R. Feng, K. Wang, X. Xu, et al., “Triple-layer optimization of distributed photovoltaic energy storage capacity for manufacturing enterprises considering carbon emissions and load management,” *Appl. Energy*, vol. 364, Art. no. 123164, 2024, doi: 10.1016/j.apenergy.2024.123164.

[5] G. Madhusudanan and P. S. Iyappan, “Enhanced energy management in microgrid system integrating photovoltaic panels, battery storage and AC grid using advanced techniques,” *Energy*, vol. 354, Art. no. 140871, 2026, doi: 10.1016/j.energy.2026.140871.

[6] W. Xiong, L. Nailiang, H. Mingkang, et al., “Risk-constrained day-ahead scheduling for gravity energy storage system and wind turbine based on IGDT,” *Renew. Energy*, vol. 185, pp. 904–915, 2022, doi: 10.1016/j.renene.2021.12.111.

[7] E. Mallada, C. Zhao, and S. Low, “Optimal load-side control for frequency regulation in smart grids,” *IEEE Trans. Autom. Control*, vol. 62, no. 12, pp. 6294–6309, 2017, doi: 10.1109/TAC.2017.2713529.

[8] L. Ren, D. Peng, D. Wang, et al., “Multi-objective optimal dispatching of virtual power plants considering source-load uncertainty in V2G mode,” *Front. Energy Res.*, vol. 10, Art. no. 983743, 2023, doi: 10.3389/fenrg.2022.983743.

[9] Y. Ma, L. Yu, G. Zhang, et al., “Source-load uncertainty-based multi-objective multi-energy complementary optimal scheduling,” *Renew. Energy*, vol. 219, Art. no. 119483, 2023, doi: 10.1016/j.renene.2023.119483.

[10] Y. Huang, M. Shahidehpour, et al., “Dual stochastic dual dynamic programming for multi-stage economic dispatch with renewable energy and thermal energy storage,” *IEEE Trans. Power Syst.*, vol. 38, no. 6, pp. 5678–5692, 2023.

[11] C. He, L. Wu, and T. Liu, “Robust co-optimization scheduling of electricity and natural gas systems via ADMM,” *IEEE Trans. Sustain. Energy*, vol. 8, no. 2, pp. 658–670, 2017, doi: 10.1109/TSTE.2016.2615104.

[12] A. Maheshwari, Y. R. Sood, and S. Jaiswal, “Flow direction algorithm-based optimal power flow analysis in the presence of stochastic renewable energy sources,” *Electr. Power Syst. Res.*, vol. 217, Art. no. 109087, 2023, doi: 10.1016/j.epsr.2022.109087.

[13] Z. Liu, H. Fan, et al., “Stochastic planning of integrated energy system based on correlation scenario generation method via Copula function considering multiple uncertainties in renewable energy sources and demands,” *IET Renew. Power Gener.*, vol. 17, no. 12, pp. 2978–2996, 2023, doi: 10.1049/rpg2.12805.

[14] C. Liu, C. Lee, H. Chen, et al., “Stochastic robust mathematical programming model for power system optimization,” *IEEE Trans. Power Syst.*, vol. 31, no. 1, pp. 821–822, 2016, doi: 10.1109/TPWRS.2015.2394320.

[15] Y. Liu, L. Wu, and J. Li, “A fast LP-based approach for robust dynamic economic dispatch problem: A feasible region projection method,” *IEEE Trans. Power Syst.*, vol. 35, no. 5, pp. 4116–4119, 2020, doi: 10.1109/TPWRS.2020.3004058.

[16] W. Liu, M. Fu, M. Yang, et al., “A bi-level interval robust optimization model for service restoration in flexible distribution networks,” *IEEE Trans. Power Syst.*, vol. 36, no. 3, pp. 1843–1855, 2021, doi: 10.1109/TPWRS.2020.3038400.

[17] R. A. Jabr, “Distributionally robust CVaR constraints for power flow optimization,” *IEEE Trans. Power Syst.*, vol. 35, no. 5, pp. 3764–3773, 2020, doi: 10.1109/TPWRS.2020.2971684.

[18] Y. Huang, W. Huang, N. Tai, et al., “A multistage distributionally robust optimization approach for generation dispatch with demand response under endogenous and exogenous uncertainties,” *IET Gener. Transm. Distrib.*, vol. 17, no. 22, pp. 5041–5061, 2023, doi: 10.1049/gtd2.13019.

[19] W. Wang, M. Wang, X. Han, et al., “Distributionally robust transmission expansion planning considering uncertainty of contingency probability,” *J. Mod. Power Syst. Clean Energy*, vol. 9, no. 5, pp. 1136–1145, 2021.

[20] Y. Zhao, Y. Chen, et al., “An adaptive distributionally robust model for three-phase distribution network reconfiguration,” *IEEE Trans. Smart Grid*, vol. 12, no. 2, pp. 1224–1237, 2021, doi: 10.1109/TSG.2020.3030299.

[21] H. Yang, et al., “Distributionally robust chance constrained planning model for energy storage plants based on Kullback–Leibler divergence,” *Energy Rep.*, vol. 7, pp. 5203–5213, 2021, doi: 10.1016/j.egyr.2021.08.116.

[22] J. Liu, Y. Chen, C. Duan, et al., “Distributionally robust optimal reactive power dispatch with Wasserstein distance in active distribution network,” *J. Mod. Power Syst. Clean Energy*, vol. 8, no. 3, pp. 426–436, 2020, doi: 10.35833/MPCE.2019.000057.

[23] L. Yao, X. Wang, C. Duan, et al., “Data-driven distributionally robust reserve and energy scheduling over Wasserstein balls,” *IET Gener. Transm. Distrib.*, vol. 12, no. 2, p. 178, 2018, doi: 10.1049/iet-gtd.2017.0493.

[24] J. Liu, Y. Chen, C. Duan, et al., “Distributionally robust optimal reactive power dispatch with Wasserstein distance in active distribution network,” *J. Mod. Power Syst. Clean Energy*, vol. 8, no. 3, pp. 426–43, 2020, doi: 10.35833/MPCE.2019.000057.